URSI GASS 2021, Rome, Italy, 28 August - 4 September 2021

Application of the Orthogonality Sampling Method in Real-World Microwave Imaging

Seongje Chae and Won-Kwang Park*
Department of Mathematics, Kookmin University, 02707, Republic of Korea.

Abstract

The orthogonality sampling method (OSM) is a well-known non-iterative imaging/detection technique in the inverse scattering problem. In this contribution, apply the OSM for identifying small anomaly from scattering parameters. For this, we design an indicator function of OSM and discover its mathematical expression to examine the feasibility and limitation. Simulation results with real-data are exhibited.

1 Introduction

Orthogonality sampling method (OSM) is a non-iterative technique for identifying locations or outline shapes of unknown targets in inverse scattering problem [1]. Throughout several related researches, it has been examined that the OSM is fast, robust, and simple technique. Due to these reasons, the OSM has been recently extended to the various problems highly related to the microwave imaging (MI) [2, 3, 4, 5]. Based on these remarkable researches, OSM will contain several potential applications in MI.

In this research, we apply the OSM for identifying locations of small anomalies from collected scattered field $S-$parameters with single source. Notice that it is very hard to measure the scattered field $S-$parameter data when the location of an antenna which transmits and receives the signal [6, 7] so that we design another indicator function which is different from the traditional one. To explain some intrinsic properties and feasibilities of the OSM, we investigate a mathematical theory by proving that the indicator function can be expressed by an infinite series of Bessel function and antenna configuration. We then exhibit some experimental results with real-data to demonstrate the theoretical results.

2 Indicator Function of the OSM

Assume that an anomaly Σ to be imaged is located at $\mathbf{r}_\star$ in a region of interests (ROI) Ω. Throughout this paper, Σ is surrounded by $N-$different dipole antennas located at $\mathbf{d}_n$, $n = 1,2,\cdots,N$, and characterized by its dielectric permittivity and electrical conductivity at a given angular frequency $\omega = 2\pi f$. With this, we set the magnetic permeability as constant, $\mu(\mathbf{r}) \equiv \mu_\mathrm{b}$, $\varepsilon_\mathrm{b} = \varepsilon_\mathrm{rb}\cdot\varepsilon_0$ and $\varepsilon_\star = \varepsilon_{\mathrm{r}\star}\cdot\varepsilon_0$, respectively, denote the background permittivity and Σ. Conductivities σ_b and $\sigma_\star$ are defined analogously. Here, ε_0 is the vacuum permittivity. With this, we denote k be the background wavenumber that satisfies $k = \omega\sqrt{\mu_\mathrm{b}(\omega\varepsilon_\mathrm{b} + i\sigma_\mathrm{b})}$ and assume that $\omega\varepsilon_\mathrm{b} \gg \sigma_\mathrm{b}$.

The measured scattered field $S-$parameter between a transmitter m and receiver n in the existence of D can be approximated as (see [8] for instance)

$$\mathrm{S}(n,m) \approx \frac{ik^2\,\mathrm{area}(\Sigma)}{4\omega\mu_\mathrm{b}}\chi(\mathbf{r}_\star)\mathrm{E}_{\mathrm{inc}}^{(z)}(\mathbf{d}_m,\mathbf{r}_\star)\mathrm{E}_{\mathrm{inc}}^{(z)}(\mathbf{d}_n,\mathbf{r}_\star), \quad (1)$$

where $\mathrm{E}_{\mathrm{inc}}^{(z)}$ is the $z-$component of incident field $\mathbf{E}_{\mathrm{inc}}$ and χ denotes the objective function.

Let $\mathbf{d}_m$ is the location of transmitter. Then, based on the experimental setting [6], we can use the arrangement of the measurement data

$$\mathbf{V}^{(m)} = \Big(\mathrm{S}(1,m),\cdots,\mathrm{S}(m-1,m),\mathrm{S}(m+1,m),\cdots,\mathrm{S}(N,m)\Big).$$

Based on the expression (1), it is natural to test the orthogonality relation between $\mathrm{S}(n,m)$ and $\mathrm{E}_{\mathrm{inc}}^{(z)}(\mathbf{d}_n,\mathbf{r})$. With this observation, we introduce a test vector: for $\mathbf{r}\in\Omega$,

$$\mathbf{W}^{(m)} = \Big(\mathrm{E}_{\mathrm{inc}}^{(z)}(\mathbf{d}_1,\mathbf{r}),\cdots,\mathrm{E}_{\mathrm{inc}}^{(z)}(\mathbf{d}_{m-1},\mathbf{r}), \mathrm{E}_{\mathrm{inc}}^{(z)}(\mathbf{d}_{m+1},\mathbf{r}),\cdots,\mathrm{E}_{\mathrm{inc}}^{(z)}(\mathbf{d}_N,\mathbf{r})\Big),$$

and design an indicator function $f_{\mathrm{OSM}}(\mathbf{r},m)$ of OSM as

$$f_{\mathrm{OSM}}(\mathbf{r},m) = \mathbf{V}^{(m)}\cdot\overline{\mathbf{W}^{(m)}} = \left|\sum_{n=1,n\neq m}^{N}\mathrm{S}(n,m)\overline{\mathrm{E}_{\mathrm{inc}}^{(z)}(\mathbf{d}_n,\mathbf{r})}\right|.$$

Then, on the basis of the orthogonality relation between $\mathbf{V}^{(m)}$ and $\mathbf{W}^{(m)}$, the maximum value of $f_{\mathrm{OSM}}(\mathbf{r},m)$ will appear at $\mathbf{r} = \mathbf{r}_\star \in \Sigma$ thereby it will be possible to identify the location of Σ. However, with this explanation, we cannot explain the phenomena that appear in the experimental results. The following result shows the feasibility of the OSM and explains the appearance of several artifacts in the map of $f_{\mathrm{OSM}}(\mathbf{r},m)$.

Theorem 2.1. *Let* $|\mathbf{d}_n| = R$, $\theta_n = \mathbf{d}_n/|\mathbf{d}_n| = (\cos\theta_n,\sin\theta_n)$, *and* $\mathbf{r}-\mathbf{r}_\star = |\mathbf{r}-\mathbf{r}_\star|(\cos\phi_\star,\sin\phi_\star)$. *If* $|k(\mathbf{d}_n-\mathbf{r})| \gg 0.250$,

$f_{\mathrm{OSM}}(\mathbf{r},m)$ *can be represented as follows:*

$$f_{\mathrm{OSM}}(\mathbf{r},m) = \left| \frac{ik(N-1)\,\mathrm{area}(\Sigma)}{32R\omega\mu_{\mathrm{b}}\pi}\chi(\mathbf{r}_\star)\mathrm{E}^{(z)}_{\mathrm{inc}}(\mathbf{r}_\star,\mathbf{d}_m) \times \left(J_0(k|\mathbf{r}-\mathbf{r}_\star|) + \frac{1}{N-1}\sum_{n=1,n\neq m}^{N} \Lambda(k,n) \right) \right|,$$

where

$$\Lambda(k,n) = \sum_{s=-\infty,s\neq 0}^{\infty} i^s J_s(k|\mathbf{r}-\mathbf{r}_\star|)\exp\left(is(\theta_n-\phi_\star)\right).$$

3 Experimental Results

Here, experimental results with real-data are exhibited. We placed $N=16$ dipole antennas equally distributed on a circle with radius of 0.090 m and applied $f=925$ MHz. Ω was selected as a circle with radius of 0.080 m.

Figure 1 shows maps of $f_{\mathrm{OSM}}(\mathbf{r},m)$ with various m. Based on the results, the imaging performance is significantly depending on the location of transmitter. Roughly speaking, the location of anomaly can be identified when the transmitter is close to the anomaly ($m=13$ or $m=16$), but it seems impossible to identify the location of anomaly when the transmitter is not close to the anomaly ($m=4$ or $m=7$).

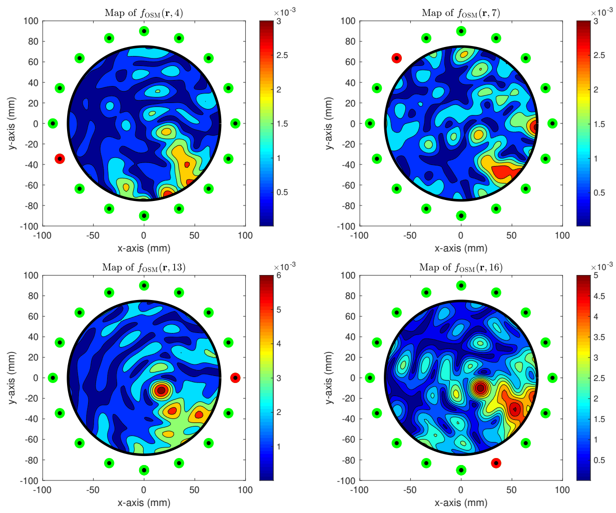

Figure 1. Maps of $f_{\mathrm{OSM}}(\mathbf{r},m)$.

Now, let us apply OSM for identifying multiple anomalies with different sizes. Opposite to the identification of single anomaly, it seems impossible to recognize the location of anomalies via the map of $f_{\mathrm{OSM}}(\mathbf{r},m)$ for any m, refer to Figure 2. Hence, further improvement is needed.

4 Acknowledgements

The authors acknowledge Kwang-Jae Lee and Seong-Ho Son for providing scattered field $S-$parameter data. This research was supported by the National Research Foundation of Korea (NRF) grant funded by the Korea government (MSIT) (No. NRF-2020R1A2C1A01005221).

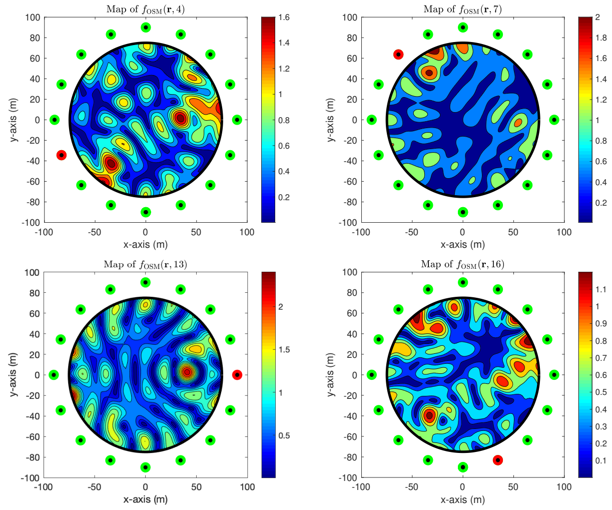

Figure 2. Maps of $f_{\mathrm{OSM}}(\mathbf{r},m)$.

References

[1] R. Potthast, "A study on orthogonality sampling," *Inverse Prob.*, vol. 26, p. Article No. 074015, 2010.

[2] M. N. Akinci, M. Çayören, and İ. Akduman, "Near-field orthogonality sampling method for microwave imaging: theory and experimental verification," *IEEE Trans. Microwave Theory Tech.*, vol. 64, no. 8, pp. 2489–2501, 2016.

[3] M. N. Akinci, "Improving near-field orthogonality sampling method for qualitative microwave imaging," *IEEE Trans. Antennas Propag.*, vol. 66, no. 10, pp. 5475–5484, 2018.

[4] M. T. Bevacqua, T. Isernia, R. Palmeri, M. N. Akinci, and L. Crocco, "Physical insight unveils new imaging capabilities of orthogonality sampling method," *IEEE Trans. Antennas Propag.*, vol. 68, no. 5, pp. 4014–4021, 2020.

[5] S. Chae, C. Y. Ahn, and W.-K. Park, "Localization of small anomalies via orthogonality sampling method from scattering parameters," *Electronics*, vol. 9, no. 7, p. Article No. 1119, 2020.

[6] J.-Y. Kim, K.-J. Lee, B.-R. Kim, S.-I. Jeon, and S.-H. Son, "Numerical and experimental assessments of focused microwave thermotherapy system at 925 MHz," *ETRI Journal*, vol. 41, no. 6, pp. 850–862, 2019.

[7] S.-H. Son, K.-J. Lee, and W.-K. Park, "Application and analysis of direct sampling method in real-world microwave imaging," *Appl. Math. Lett.*, vol. 96, pp. 47–53, 2019.

[8] M. Haynes, J. Stang, and M. Moghaddam, "Real-time microwave imaging of differential temperature for thermal therapy monitoring," *IEEE Trans. Biomed. Eng.*, vol. 61, no. 6, pp. 1787–1797, 2014.